Aeronautical Research Institute, University of Tokyo
Report No. 342, April 1959

Experimental Investigation of Transonic Flow Past Two-Dimensional Biconvex Circular-Arc Airfoils at Small Angles of Attack

By

Ryuma KAWAMURA and Keiichi KARASHIMA

Summary. In this paper are presented the results of an experimental investigation of transonic flows past biconvex circular-arc airfoils with thickness-chord ratios of 10.6, 8.08 and 5.44 percent. Aerodynamic characteristics of the airfoils are analysed from the surface pressure distributions obtained by interferometry. It is found that most of the experimental results confirm the validity of the transonic similarity rule while there are some such as position of the surface shock which are not well arranged by means of the similarity rule. It is also turned out that the lift coefficient is not exactly proportional to the angle of attack even at the origin near Mach number one. The result on the detached shock location at low supersonic Mach numbers seems to give an experimental evidence to Busemann's analysis to the transonic flow with detached shock.

1. INTRODUCTION

In the theory of transonic inviscid flow, the difficulty with which we are confronted at the first step is the non-linearity of the basic equation in the physical plane even under the assumption of small perturbation flow. In case of two-dimensional flow, however, it is possible in general to reduce the equation to linear one by the use of hodograph method. The transonic small perturbation equation thus obtained is of the simplest mixed type and called the Tricomi equation. The greater part of the analytical treatments of the transonic flow around thin bodies developed so far has been done in success by adopting the hodograph method. Unfortunately, in the treatment of the flow in the hodograph plane, there arises another difficulty that the boundary conditions cannot be prescribed except for special cases [*1*]. For this reason, application of the hodograph method to two-dimensional transonic theory seems to be limited to the flow around very simple bodies such as wedge sections, in which the hodograph boundary condition can exceptionally be fixed *a priori*.

In these circumstances, it may be the natural trend to give up the hodograph method and try to find other routes to access the solution for general shaped bodies. Recently, some approximate methods have been developed along this line, in which the problem is entirely treated in the physical plane. These are the integral equation method [*2*] [*3*] and the local linearization method [*4*] [*5*] both originated

by Oswatitsch and extended by Spreiter and others. The results obtained by these methods seem to be fairly good and be able to afford practical applications, though they are much inferior to the hodograph method in mathematical exactness.

On the other hand, in the experimental side, there are not so many available data on the present problem. This is especially so for general shaped bodies other than wedge sections. The accumulation of the experimental data about wedge sections are now fairly complete except for the lifting case and the comparison of them with the theories shows satisfactory agreement in general.

However, quite a few experimental investigations seem to have been done so far on the transonic flow around two-dimensional bodies with curved surface. The situation is such that we may have some trouble when we will try to check the new theory by the experiment on these problems. It is doubtless that detailed experimental investigations on this problem will help the progress of the transonic theory.

The present study has been arranged with the intention to supplement the lack of the experimental data for bodies with curved surface as mentioned above. For the sake of simplicity in production of the models and also in analysis of the results, symmetrical circular-arc airfoils are chosen as the models. The aerodynamic characteristics of the models and detailed flow phenomena have been investigated by means of Mach-Zehnder interferometer. The same kind of experiment was done by Bryson [*6*] in 1952. At that time, he used a fixed-wall wind tunnel, and hence, could not extend the experiment over the range of Mach number very close to unity, in which applicability of transonic theory is ensured most. In view of this fact, a transonic wind tunnel with slotted walls was used in the present experiment and emphasis was laid on obtaining the results in this Mach number range. Since the scale of the wind tunnel was very small, and accordingly, Reynolds number of the experiment was impractically low, the effect of the laminar separation behind the surface shock wave was comparatively large and a part of the experimental results cannot be applied directly to practical problems or to comparison with the inviscid theory. Even in such cases close examination of the flow and deep comprehension of the viscous phenomena will give us a correct interpretation of the experimental results. Moreover, there were still a great deal of results substantially not influenced by the viscous effects.

The description of the experiment and its results will be given in the following sections.

2. Experiment

2.1 *Wind Tunnel*

A small scale transonic wind tunnel with a 40 mm by 94 mm rectangular test section was used throughout the present experiment. The side walls (94 mm in height) are made of solid plate with glass window (100 mm in diameter) in its central part, while the top and the bottom walls (40 mm in breadth) consist of plate with three line slots. The opening ratio of the slotted walls is 10 percent. The

main part of the wind tunnel is shown in Fig. 1. It is connected to a 75 HP vacuum pump, by which atmospheric air is blown into the wind tunnel. A big capacity

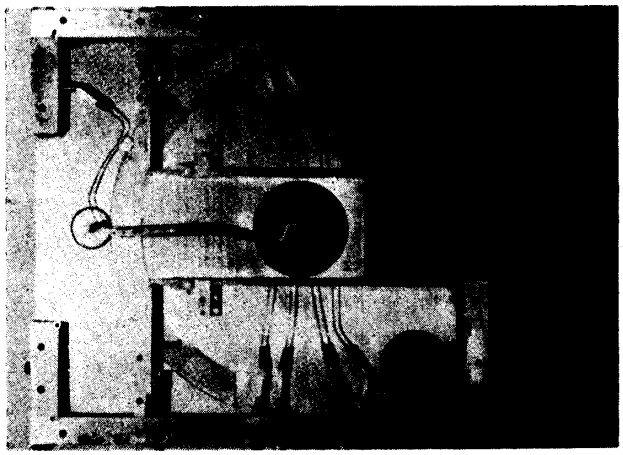

FIGURE 1. Wind tunnel (one side wall is removed).

vacuum tank ($300\,m^3$) between the tunnel and the pump makes the running time of the tunnel sufficiently long for the present purpose. A silica-gel air dryer is installed at the entrance of the wind tunnel in order to avoid water condensation.

There are plenum chambers outside the top and bottom walls. At transonic Mach numbers a part of the main flow is automatically sucked into the plenum chamber through slots and thus the chocking can be avoided even at Mach number one. The air picked out of the main flow re-enters into the main passage behind the testing chamber through movable flaps, by which the amount of the suction, and hence, the Mach number at the test section are smoothly regulated.

At the beginning of the experiment, the Mach number at the vacant test section (no model) was measured by interferometry at various flap conditions and correlated to the pressure in the plenum chamber. In the experiment with a model in the test section the free stream Mach number was defined from the plenum chamber pressure such that it was the same as that obtained at the vacant test section under the same plenum chamber pressure. The highest Mach number obtained in this wind tunnel is 1.165. The uniformity of the flow is almost satisfactory at Mach numbers up to 1.10, above which it is slightly disturbed as is seen in Fig. 2.

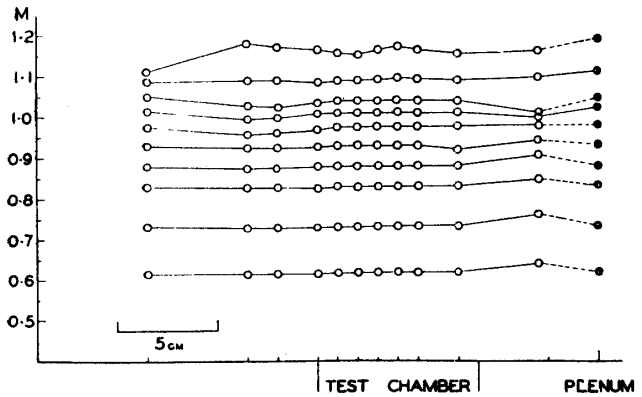

FIGURE 2. Mach number distribution in the test chamber (no model).

2.2 *Models*

Three airfoil models with symmetrical circular-arc section were prepared for the experiment. They span the breadth of the wind tunnel, their chord length is 20 mm, and the thickness-chord ratios are 0.1060, 0.0808 and 0.0544, respectively. A pressure hole at the mid-chord on the upper surface was used as a check on the measured fringe identification in the interferometry. The model is supported by

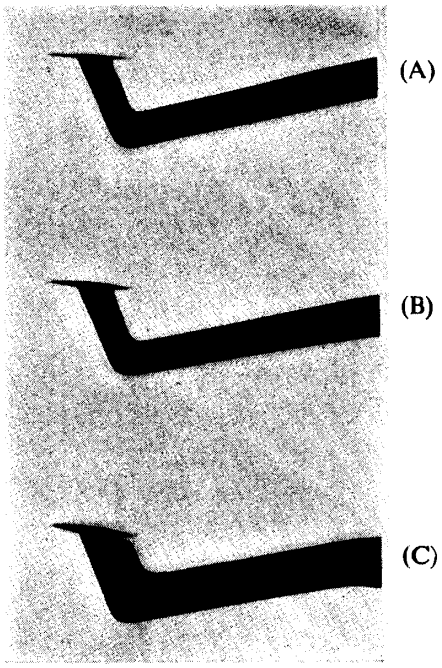

FIGURE 3. Models: (A) $\tau=0.1060$, (B) $\tau=0.0808$, (C) $\tau=0.0544$.

a cantilever sting on the lower surface as shown in Fig. 3. Precise inspection of the model shapes indicated that the error in thickness was smaller than one percent except for the inevitable rounding-off at the sharp leading and trailing edges. Thickness of the models at these edges was the order of 0.006 mm, approximately.

2.3 *Method of Experiment*

In this experiment most of the measurements were made using a Mach-Zehnder

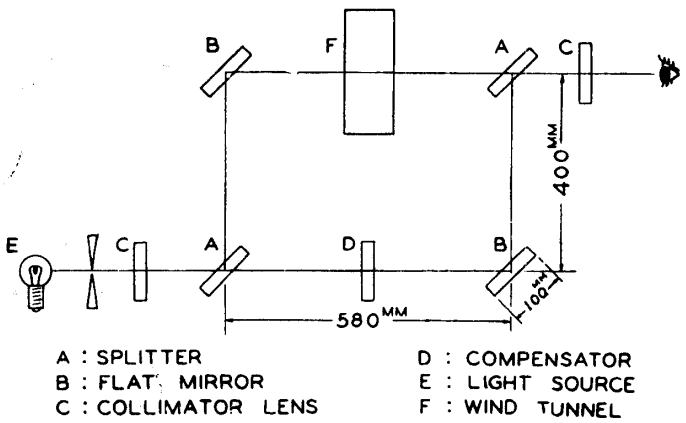

FIGURE 4. Diagram of Mach-Zehnder interferometer.

interferometer illustrated in Fig. 4. As the light source, use was made of an exciter lamp for white light and a high-pressure mercury lamp which, in combination with a neodymium glass filter, produced monochromatic light of 5463 Å wave length. The white light was used for the center fringe identification.

The density in the flow field was calculated from the interferogram in the ordinary way according to the following formula:

$$\rho_0-\rho=\frac{1}{K}\frac{\lambda}{L}\varepsilon, \quad \varepsilon=\frac{l}{d}, \tag{1}$$

where ρ is the density, K the Goldstone-Dale constant, λ the wave length of the monochromatic light, L the effective breadth of the test section, and ε the number of the fringe shift, that is, the distance, l, shifted by a fringe in passing from the no-wind state to the measured one divided by the distance, d, between the neighbouring fringes. The subscript 0 denotes no-wind condition.

The length L in Eq. (1) should be shorter than the geometrical breadth of the test section because of the boundary layer growth on the side walls. It was determined in such a way that the density in the test section without model calculated from interferometry by using Eq. (1) coincided with the value obtained from pressure measurement by the use of isentropic relations. The value of the effective breadth thus obtained is 38.84 mm instead of the geometrical length of 40 mm and was used as a constant throughout the present experiment. This value seems to be reasonable in view of the boundary layer growth.

Thus, the constant values used in Eq. (1) are as follows:

$$K=2.222\times10^{-3}\ \mathrm{kg^{-1}\,s^{-2}\,m^4},$$
$$\lambda=5463\ \text{Å},$$
$$L=0.03884\ \mathrm{m}.$$

Since, as mentioned previously, the models were supported by a cantilever sting which shaded a part of the lower flow field in the interferogram, only the upper field was available for interferometry. However, owing to the symmetry of the model section, it is possible to assume that the flow field in the lower side at an angle of attack, α, is the same as that in the upper side at an angle of attack, $-\alpha$, at the same free stream condition. On this assumption the aerodynamic characteristics were obtained from the measurements only in the upper flow fields in the present experiment. Since the models were too thin to drill two pressure holes symmetrically on both surfaces, it was impossible to determine zero angle of attack by the usual procedure of pressure comparison. In this experiment, zero angle of attack setting was made by the trial-and-error method so as to make the fringe shift symmetric on the upper and lower surfaces in the forward part of the model.

2.4 *Range Covered in the Experiment*

In this experiment, Mach number range was from 0.790 to 1.165 and the measurements were made at small intervals of the free stream Mach number especially near Mach number one. Reynolds number in reference to the chord length was the order of 10^4. It varies with Mach number in this type of wind tunnel. The

relation between Mach number and Reynolds number in this experiment is given in Fig. 5. The angle of attack was limited to relatively small values (0° to 2°)

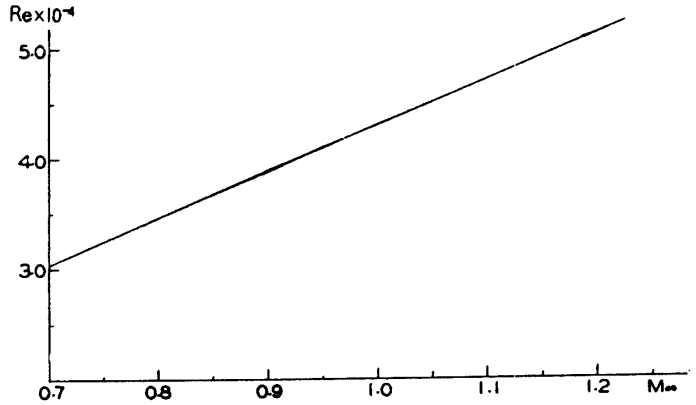

FIGURE 5. Reynolds number versus free-stream Mach number.

because of the severe leading edge separation and also of the uncertainty of the wall interference at large angles of attack.

3. Results of the Experiment

3.1 *Representation of the Results*

Experimental results are mostly arranged by parametric representations according to the transonic similarity rule proposed by Spreiter [7] [8]. The definitions of the transonic parameter and the reduced coefficients are shown below:

1) Transonic similarity parameter

$$\xi_\infty = \frac{M_\infty^2 - 1}{[(\gamma+1)\tau]^{\frac{2}{3}}},$$

2) Reduced pressure coefficient

$$\tilde{C}_p = \frac{(\gamma+1)^{\frac{1}{3}}}{\tau^{\frac{2}{3}}} C_p,$$

3) Reduced lift coefficient

$$\tilde{C}_L = \frac{(\gamma+1)^{\frac{1}{3}}}{\tau^{\frac{2}{3}}} C_L,$$

4) Reduced drag coefficient

$$\tilde{C}_D = \frac{(\gamma+1)^{\frac{1}{3}}}{\tau^{\frac{5}{3}}} C_D,$$

5) Reduced pitching-moment coefficient

$$\tilde{C}_m = \frac{(\gamma+1)^{\frac{1}{3}}}{\tau^{\frac{2}{3}}} C_m,$$

6) Reduced lift-curve slope

$$\left[\frac{d\tilde{C}_L}{d\alpha}\right]_{\alpha=0} = [(\gamma+1)\tau]^{\frac{1}{3}} \left[\frac{dC_L}{d\alpha}\right]_{\alpha=0},$$

7) Reduced pitching-moment-curve slope

$$\left[\frac{d\tilde{C}_m}{d\alpha}\right]_{\alpha=0}=[(\gamma+1)\tau]^{\frac{1}{3}}\left[\frac{dC_m}{d\alpha}\right]_{\alpha=0},$$

where γ is the ratio of specific heats, τ the thickness-chord ratio of the model, M_∞ the free stream Mach number and α the angle of attack, respectively. The areodynamic coefficients are expressed in the usual manner and the barred quantities denote the reduced ones.

3.2 *General Character of the Flow Field*

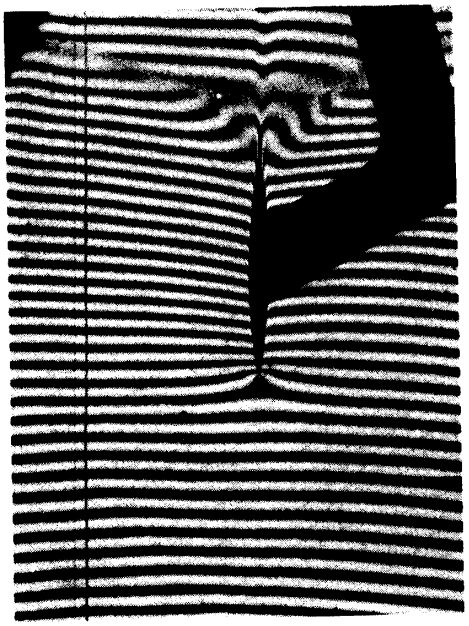

FIGURE 7. Finite fringe interferogram; $M_\infty=0.999$, $\tau=0.0308$, $\alpha=0°$.

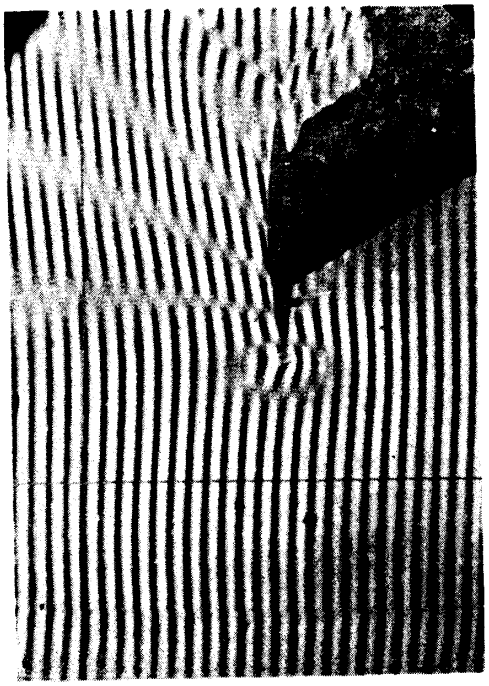

FIGURE 9. Superposed finite fringe interferogram; $M_\infty=1.085$, $\tau=0.1060$, $\alpha=0°$.

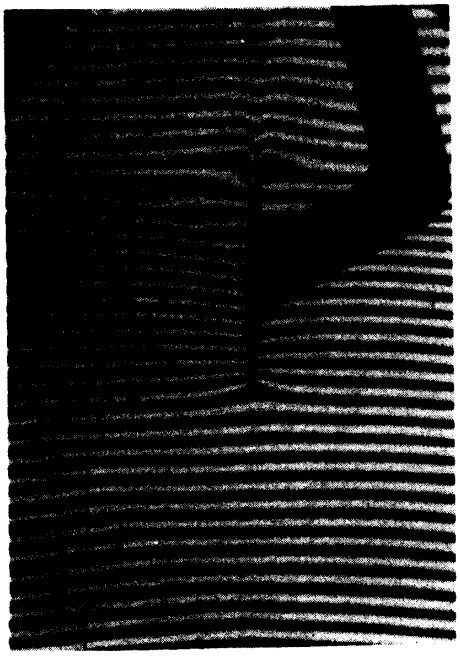

FIGURE 6. Finite fringe interferogram; $M_\infty=0.911$, $\tau=0.0808$, $\alpha=0°$.

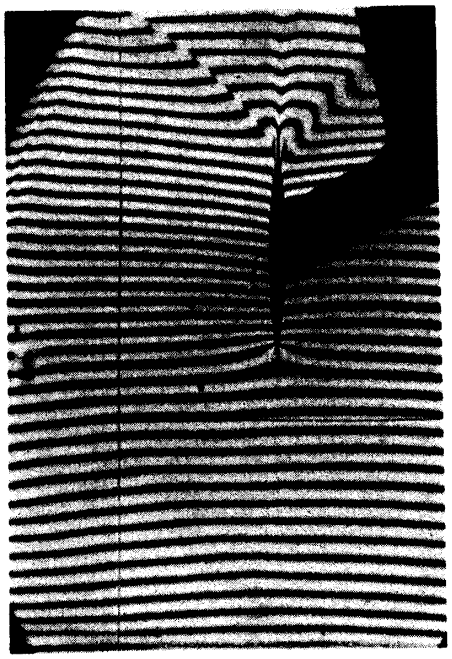

FIGURE 8. Finite fringe interferogram; $M_\infty=1.122$, $\tau=0.0808$, $\alpha=0°$.

Figs. 6 to 8 show typical interferograms of the flow field around the 8.08 percent circular-arc airfoil at zero angle of attack and at Mach number close to one taken by means of finite fringe method. In Fig. 9 is shown an example of superposed finite fringe interferogram of the 10.6 percent airfoil in which lines of constant density appear very clearly. The former type of interferogram was used for the evaluation of the surface pressure distribution and the latter for the analysis of the flow field. A calculated flow field corresponding to Fig. 9 is shown in Fig. 10

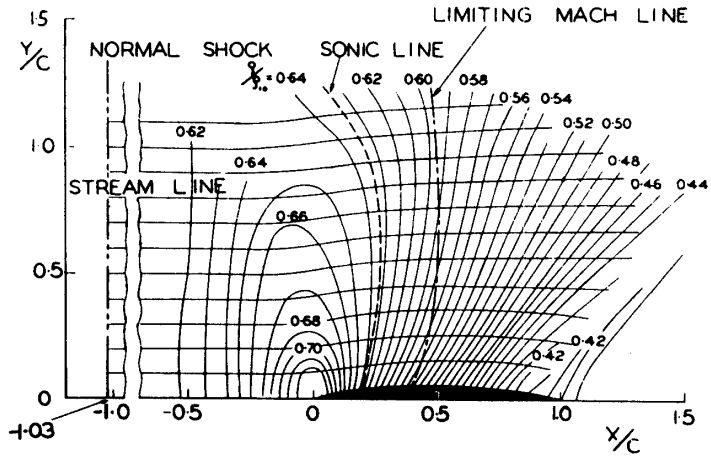

FIGURE 10. Calculated flow field; $M_\infty=1.085$, $\tau=0.1060$, $\alpha=0°$.

in which are drawn equidensity lines, stream lines, sonic line, limiting Mach line and detached shock. ρ_{10} in the figure denotes the stagnation density ahead of the detached shock nearly normal to the free stream. In these figures it is noticeable that the equidensity lines are almost straight near the body except in the narrow region around the leading edge. This clearly shows a characteristic feature of the transonic flow that lateral extension of the disturbances is very large compared with longitudinal one.

Typical Schlieren photographs are shown in Fig. 11 in which are seen the variation of the shape and position of the surface shock with free stream Mach number. A λ-shock and accompanied severe separation of the laminar boundary layer are clearly seen in Fig. 11 (B). A normal shock appears behind the trailing edge at Mach number very close to one as shown in Fig. 11 (C).

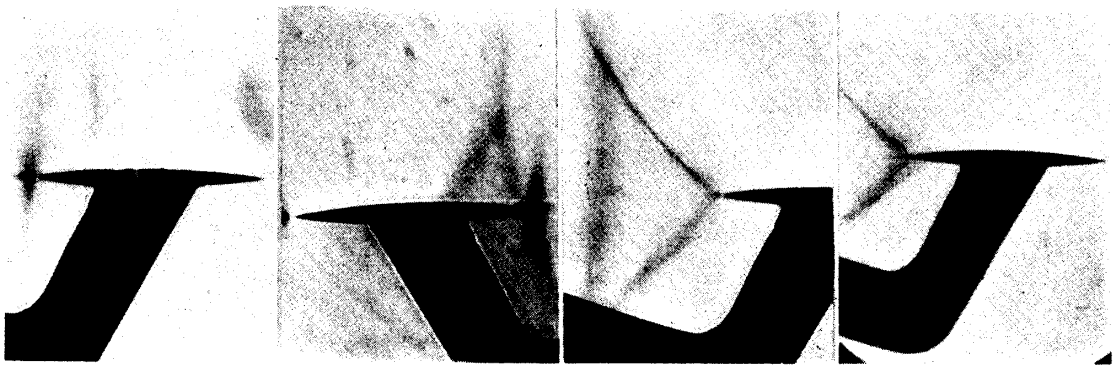

(A) $M_\infty=0.861$ (B) $M_\infty=0.894$ (C) $M_\infty=0.999$ (D) $M_\infty=1.087$

FIGURE 11. Schlieren photographs; $\tau=0.0808$, $\alpha=0°$.

3. 3 *Pressure Distribution*

Pressure distributions on the biconvex circular-arc airfoils at zero angle of attack are shown in Figs. 12 to 14. Position of the sonic point is also marked on each curve in the figures whenever it appears. The pressure coefficient C_p was calculated from the density outside the boundary layer by the isentropic relation.

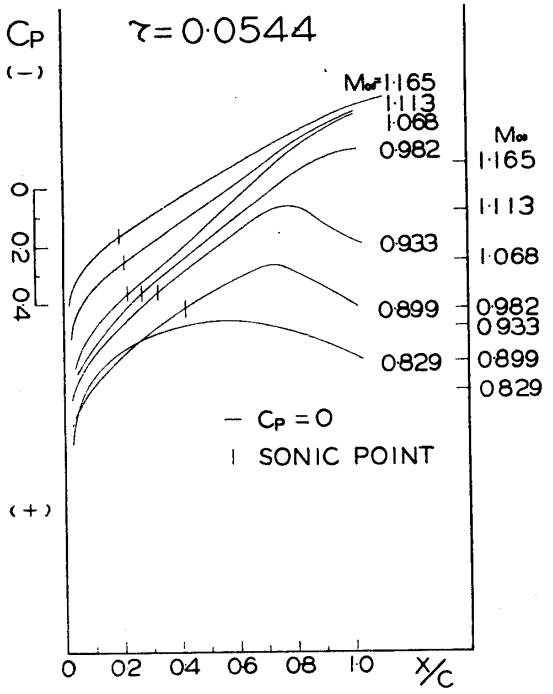

FIGURE 12. Pressure distributions at zero incidence.

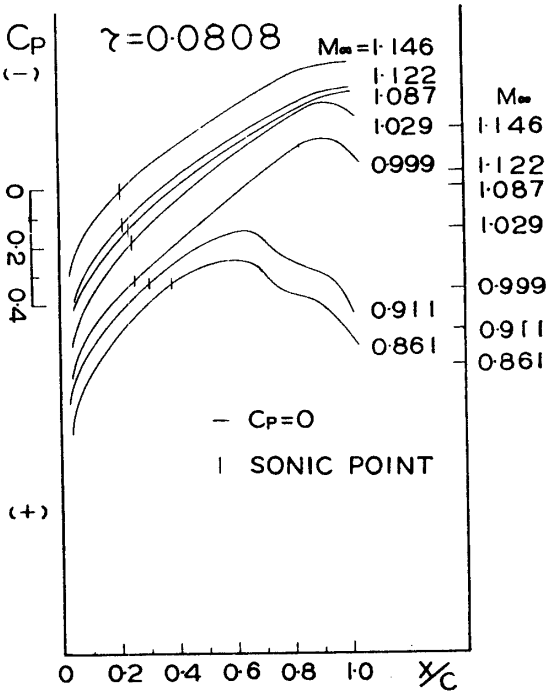

FIGURE 13. Pressure distributions at zero incidence.

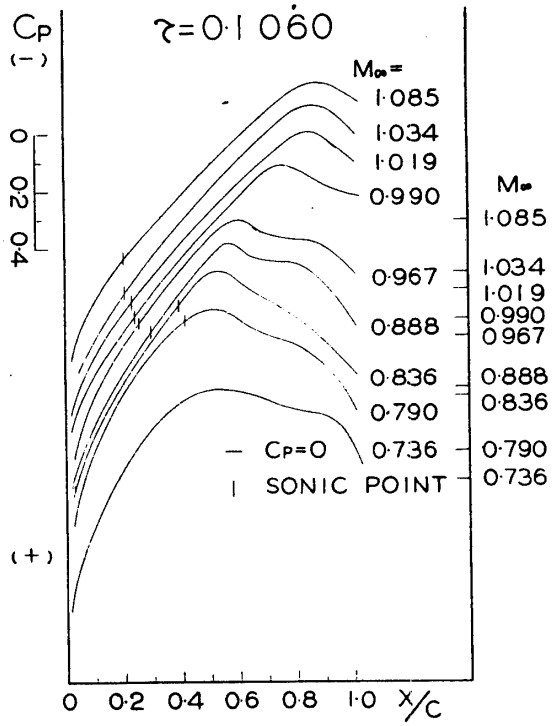

FIGURE 14. Pressure distributions at zero incidence.

At supersonic Mach numbers at which detached shock appears ahead of the leading edge, change of the stagnation pressure was taken into accounts according to the normal shock condition. Modification of the isentropic relation due to the surface shock at supercritical Mach numbers was neglected because of the reasons that the exact condition of the shock wave was not certain from the interferogram and also that the shock strength must be very weak in any case.

Since Reynolds number was very small in the present experiment, laminar separation occured as soon as the region of increasing pressure was reached. The pressure distribution in the down stream part of the separation, especially behind the surface shock, is unable to be compared with other experimental results obtained at moderate or large Reynolds numbers. However, rearward movement of the surface shock with increasing Mach number is very rapid and the effects of the separation is restricted to the narrow region near the trailing edge above a certain high supercritical Mach number. In such cases viscous effects on the aerodynamic characteristics of the airfoil are small.

In the transonic theory it is already known that freezing of the flow field is realized at the free stream Mach number one, and as a result, distribution of local Macn number M on the body surface is kept stationary at $M_\infty=1$, namely,

$$\left[\frac{dM}{dM_\infty}\right]_{M_\infty=1}=0.$$

Fig. 15 shows the local Mach number distribution on the 10.6 percent airfoil at the free stream Mach number very close to one. In the figure it is seen that all experimental points except for those at $M_\infty=0.963$ fall well on one curve. The same tendency was found in the results of the other two airfoils. Hence, it can be said that stationary state of local Mach number at $M_\infty=1.00$ is well established by the experiment and it holds in comparatively narrow range of M_∞.

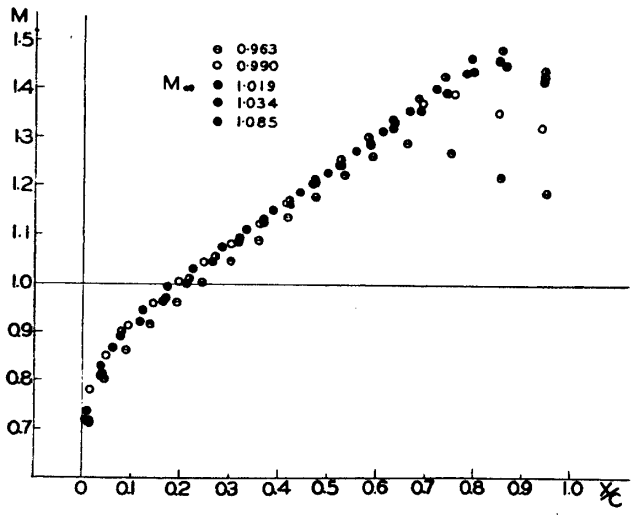

FIGURE 15. Local Mach number distributions near free-stream Mach number one; $\tau=0.1060$, $\alpha=0°$.

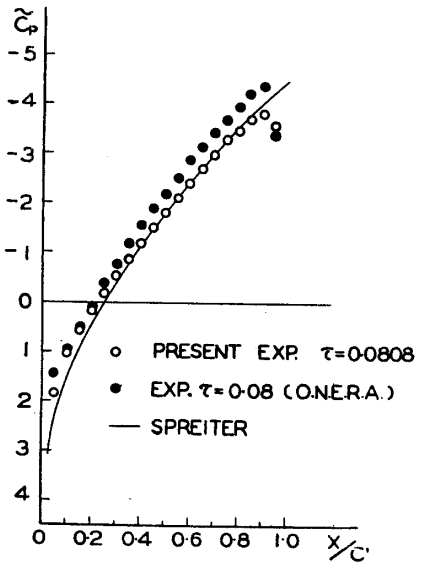

FIGURE 16. Pressure distributions at $M_\infty=1.00$, $\alpha=0°$.

A comparison of theoretical and experimental pressure distributions at $M_\infty = 1.00$ is given in Fig. 16, in which white marks indicate the results of the present experiment for the 8.08 percent airfoil, black marks for 8 percent circular-arc airfoil obtained at ONERA, and solid line is the theoretical results by Spreiter [5]. The present experiment shows better agreement with Spreiter's theory than that at ONERA. Also in Fig. 17 is shown a comparison of the variation of the pressure coefficient at mid-chord of circular-arc sections with Mach number in terms of the transonic similarity representation. In view of the large scattering of the experimental points in the domain of small ξ_∞, the lower limit of the range in which the transonic similarity rule can hold at least for the mid-chord pressure seems to be about $\xi_\infty = -0.5$. The agreement of Spreiter's theory with the experiments is not good at all.

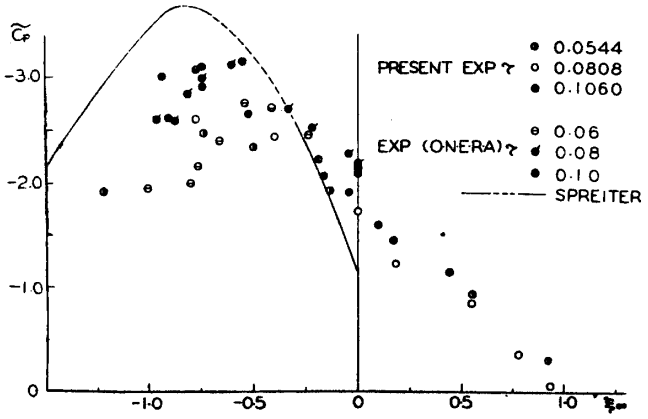

FIGURE 17. Variation of reduced pressure coefficient at mid-chord of circular-arc airfoils with transonic similarity parameter.

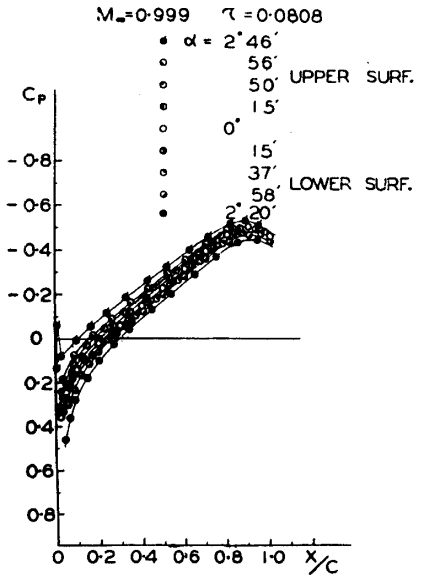

FIGURE 18. Variation of pressure coefficient with angle of attack.

A typical example of variation of surface pressure distribution with angle of attack at Mach number nearly equal to one is presented in Fig. 18. At small angles of attack below 2.5° the distributions on the upper and the lower surfaces deviate almost symmetrically from zero-incidence curve, while at large angles of attack, a suction pressure peak appears on the upper surface in the vicinity of the leading edge clearly caused by a rapid expansion of the flow around the sharp leading edge. The expansion zone terminates at an oblique shock and seems to have negligible influence on the downstream pressure distribution. The expansion region is so narrow that exact evaluation of the pressure there is hard to get from the interferogram.

3.4 *Lift Coefficient and Lift-Curve Slope*

Lift coefficient is easily calculated from pressure distribution by integration. In the experiment, special attention was paid to the behaviour of C_L–α curve at Mach number one. A typical example is presented in Fig. 19 in which experi-

mental result for NACA 64-A-010 airfoil obtained by Michel and Sirieix [9] is plotted for comparison. The slope of the C_L–α curves in the present experiment are slightly smaller at $\alpha=0$ than that of NACA 64-A-010 airfoil. Furthermore, it is remarkable in Fig. 19 that the C_L–α curves of the circular-arc airfoils are not straight and their slope decreases with increasing angle of attack. Closer examination of the experimental results shows the fact that it is caused by the more

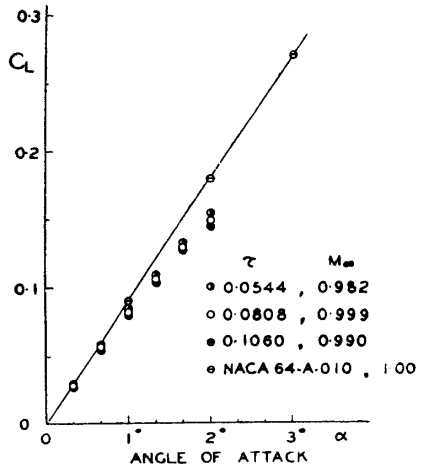

FIGURE 19. Variation of lift coefficient with angle of attack near Mach number one.

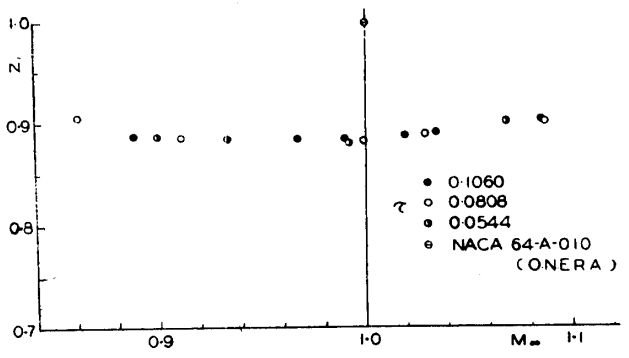

FIGURE 20. Variation of power index of α with free-stream Mach number.

gradual change of suction on the upper surface as a whole than on the lower one in spite of the appearance of the expansion zone near the leading edge at angles of attack. It is not so curious that the C_L–α curve is not straight since the transonic similarity rule foretells us the fact that C_L should be proportional not to α but to $\alpha^{\frac{2}{3}}$ at Mach number one. Assuming the proportionality of C_L to α^n, the power index n is easily obtained from the slope of C_L–α curve on a logarithmic diagram. Variation of n thus obtained with M_∞ is shown in Fig. 20. The value of n is about 0.90 in the vicinity of $M_\infty=1$ and seems to approach one as M_∞ decreases.

The lift-curve slopes obtained by the experiment are plotted in Fig. 21 in the transonic similarity representation together with other theoretical and experimental results for double-wedge airfoils. It is seen from the figure that the experimental results are well arranged in one curve over the range of the experiment. The fact that the present results agree with the theoretical ones for double-wedge airfoils obtained by Vincenti and Wagoner [10] at low supersonic range where the viscous effect has little influence on the flow field may suggest that change of airfoil shape might have only secondary effect on the lift problem in this Mach number range. The well-arrangement of the experimental points and their smooth continuation to those of double-wedge airfoil obtained by Solomom and Willmarth [11] in the range below $\xi_\infty=-0.5$ seem to be rather incidential, since the effect of boundary layer separation is very large here. The value of the reduced lift-curve slope at $\xi_\infty=0$ is about 3.0 for the circular-arc airfoils in the present

experiment and is slightly smaller in comparison with the experimental value for NACA 64-A-010 by Michel and Sirieix and the theoretical value of 3.3 for double-wedge airfoil by Guderley and Yoshihara [*12*].

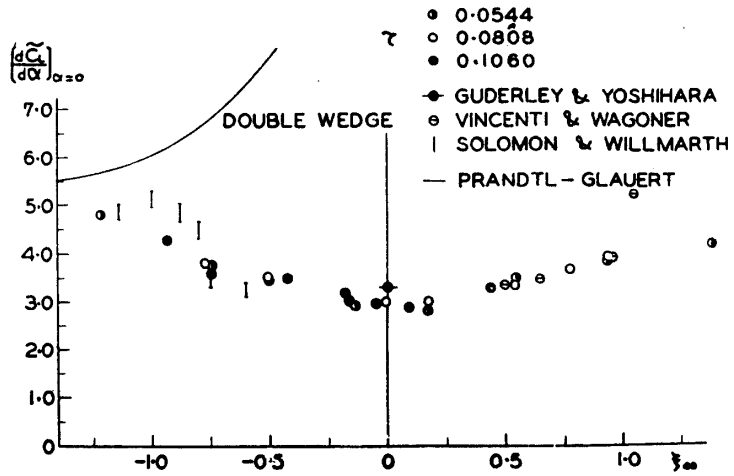

FIGURE 21. Variation of lift-curve slope at zero incidence versus transonic similarity parameter.

The stationary state of the flow at $M_\infty=1$ is again confirmed by the experimental data shown in Fig. 21 in which $(dC_L/d\alpha)_{\alpha=0}$ is nearly constant in the vicinity of $\xi_\infty=0$.

3. 5 *Drag Coefficient*

Drag coefficient C_D was calculated from surface pressure distribution obtained by the experiment. Therefore, frictional drag is not included in C_D in this paper. Variation of reduced drag coefficient of the circular-arc airfoils at zero angle of attack with transonic similarity parameter ξ_∞ is presented in Fig. 22 together with experimental results by Bryson [*6*] and ONERA group and theoretical curves by Spreiter [*3*] [*5*] for the same kind of airfoils. The experimental points obtained in the present experiment and at ONERA are well arranged in one curve in the low supersonic region showing the correctness of the transonic similarity rule. It

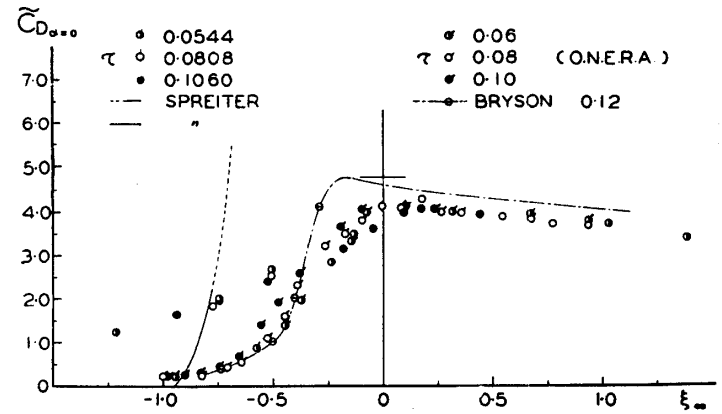

FIGURE 22. Variation of drag coefficient at zero incidence versus transonic similarity parameter.

must be noticed that, in this Mach number range, viscous effect on the flow field is minimized due to the retardation of the surface shock to the trailing edge and prevalence of accerlerating flow almost over the whole surface. On the other hand, in Fig. 22, there are remarkable discrepancies between the results of the present and the other experiments. This is obviously caused by the difference of Reynolds number of the experiments. As has been already mentioned in 3.3, laminar boundary layer separation occured inevitably in this experiment even at subcritical Mach numbers because of the small Reynolds number, and accordingly, drag due to pressure became much higher than those obtained at moderate Reynolds numbers. Though the separation of the boundary layer becomes severer by the interaction with the surface shock in the supercritical region, its effect on the aerodynamic characteristics of the airfoil reversely diminishes as Mach number increases because of the reason that the separation point moves quite rapidly towards the trailing edge as the shock with increasing Mach number thus narrowing the domain of the surface influenced by the separation. In the high Reynolds number experiment without initial laminar separation as in the cases of Bryson [6] and ONERA, the rapid rearward movement of the shock usually results in a sharp rise of drag coefficient with increasing Mach number beyond the critical value. In the present experiment, however, the sharp rise of drag coefficient in supercritical region is almost smoothed out by its large value in subcritical region due to the laminar separation. At high subsonic Mach numbers close to one the shock attaches to the trailing edge and the effect of the separation is quite restricted to the very vicinity of the trailing edge. Hence, the experimental results should agree with the transonic similarity rule as is actually seen in Fig. 22. The deviation of the experimental point by Bryson at $\xi_\infty = -0.25$ from those of the present and ONERA experiments may be caused by the large thickness of his airfoil.

Theoretical analyses were made by Spreiter on the drag problem of symmetrical body in transonic flow. His theory is divided into two: the one is the integral equation method appropriate to treat transonic flow with surface shock on the body in supercritical Mach number range and the other the local linearization method applicable to the flow near Mach number one. The theoretical results obtained by applying these methods to a circular-arc airfoil are shown in Fig. 22 in solid

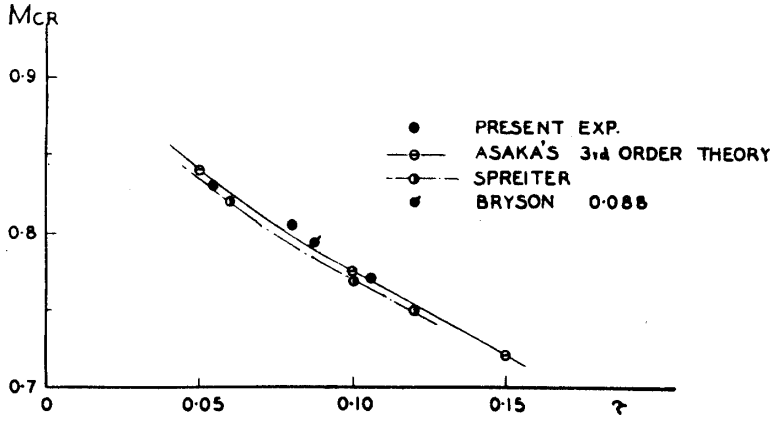

FIGURE 23. Critical Mach number versus thickness-chord ratio.

lines. It is seen that the steepness of the drag rise of the theoretical curve is far extreme compared with the experimental results even the viscous effect being taken into consideration. Since, as is seen in Fig. 23, coincidence of the theory with the experiment is very well at least on the critical Mach number, the disagreement on the rate of drag rise in Fig. 22 seems to indicate certain incompleteness of the theory in the treatment of the surface shock. The local linearization method gives a fairly nice value for the drag at Mach number one, though still a little bit higher than the experimental ones. It is certain that, even in the Mach number range around one in which the shock attaches to the trailing edge, there occurs pressure rise near the trailing edge due to the shock boundary layer interaction which has the effect of reducing the drag. On this point, Michel and others [*14*] proposed a correction method in which the pressure distribution curve on the greater part of the airfoil is extended smoothly to the trailing edge, thus replacing the pressure rise by pressure down in the vicinity of the trailing edge and cancelling the effect of the shock-boundary layer interaction. Though the method is not so strict, the resulting extrapolated drag seems to fit better than the uncorrected one to be compared with the theory. The extrapolated drag of the present experiment is shown in Fig. 24 together with Spreiter's theoretical curve. The agreement is clearly excellent.

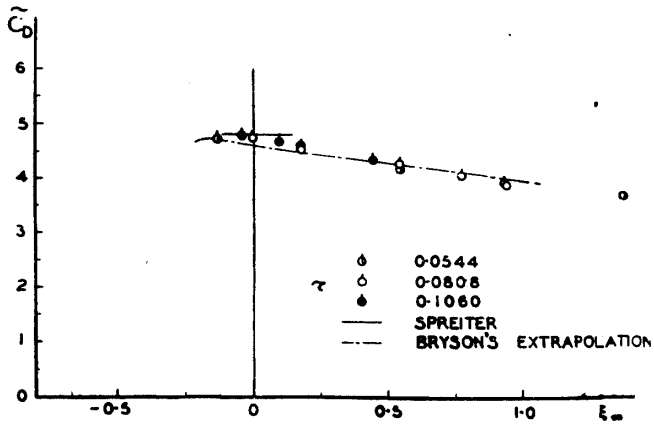

FIGURE 24. Extrapolated drag versus transonic similarity parameter.

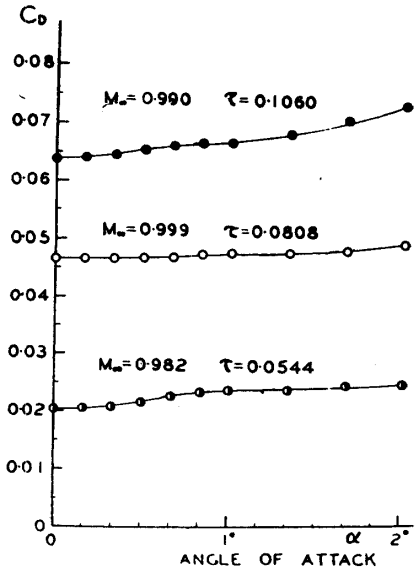

FIGURE 25. Variation of drag coefficient with angle of attack.

Fig. 25 shows typical examples of variation of drag coefficient with angle of attack near Mach number one. Examination of pressure distributions reveals that drag on the lower surface has a trend of increasing regularly with angle of attack, while on the upper surface, it decreases first slightly for small angle of attack and rapidly for large one. The rate of the drag rise on the upper surface is greater than that of the drag down on the lower surface and the resultant drag gradually increases with angle of attack as shown in Fig. 25.

3.6 *Pitching-Moment Coefficient and Position of the Centre of Pressure*

An example of variation of pitching-moment coefficient C_m around the quarter chord point from the leading edge at Mach number one with angle of attack is shown in Fig. 26, in which minus sign of C_m means head-down moment. The experimental results for NACA 64-A-010 obtained at ONERA are also plotted for comparison. Smaller values of C_m in the present experiment than at ONERA was caused by the smaller value of C_L and more forwarded position of the centre of pressure in the present experiment than in NACA 64-A-010. In Fig. 27 is shown

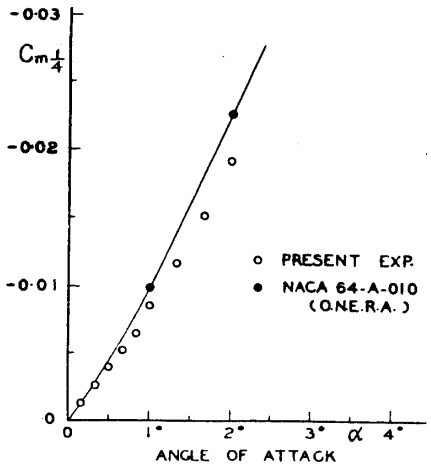

FIGURE 26. Variation of pitching-moment coefficient with angle of attack at Mach number one. $\tau=0.0808$.

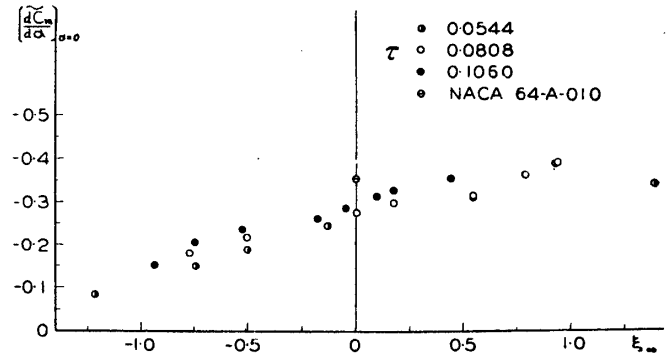

FIGURE 27. Variation of pitching-moment curve slope at zero incidence versus transonic similarity parameter.

the relation between slope of the pitching-moment curve at zero angle of attack and Mach number in transonic similarity representation. It is seen in the figure that arrangement of the experimental points in one similarity curve is not good, but appears a systematic scattering according to airfoil thickness. Distortion of pressure distribution due to the separation of boundary layer caused by small Reynolds numbers in the present experiment may be, to a certain extent, responsible for this point. In this sense, the present data on the pitching-moment are not so reliable especially in the supercritical Mach number range where the surface shock produces severe boundary layer separation.

In reference to the pitching-moment, position of the centre of pressure is another point of interests. In Figs. 28 and 29 are given variations of position of the center of pressure at Mach number one with angle of attack and at zero angle of attack with Mach number, respectively. It is seen in Fig. 29 that the experimental points for the circular-arc airfoils with different thickness fall well on one curve, thus confirming the validity of the transonic similarity rule. The centre of pressure locates at about 25 percent-chord in low Mach number range, gradually moves rearwards in supercritical range reaching about 35 percent-chord at Mach number one and does not show any further rearward movement in low supersonic range. It is well known in the linearized supersonic theory that the centre of pressure

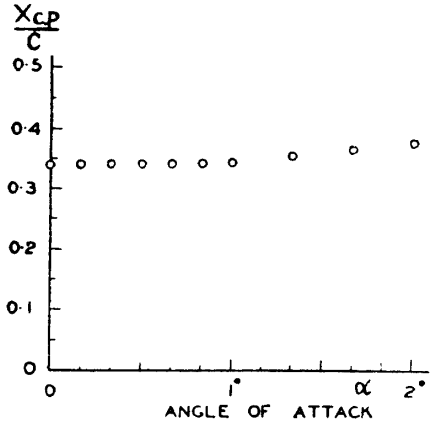

FIGURE 28. Variation of centre of pressure loca tion with angle of attack at Mach number one. $\tau=0.0808$.

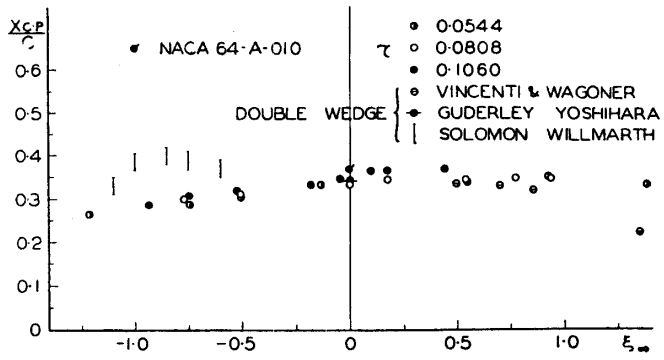

FIGURE 29. Variation of centre of pressure location at zero incidence with transonic similarity parameter.

locates nearly at 50 percent-chord in pure supersonic flow. In the present experiment, however, Mach number range could not be extended to the value, at which the bow shock attaches to the leading edge, and hence, behaviour of the centre of pressure location at high Mach numbers is uncertain from the present experiment. Position of the centre of pressure for the circular-arc airfoils at Mach number one is almost coincident with the theoretical one for double-wedge airfoil obtained by Guderley and Yoshihara and slightly forward compared with the experimental one for NACA 64-A-010.

3. 7 *Position of the Shock Wave on the Airfoil Surface*

The surface shock was observed by means of Schlieren method. It appears first in the flow field at Mach number slightly higher than the critical value. At the first stage, it is almost a normal shock and does not produce severe separation of the boundary layer. As the free-stream Mach number increases, the surface shock moves rearward and increases its strength rapidly, thus changing its shape into the form of λ as a result of shock-boundary layer interaction. It reaches the trailing edge at Mach number slightly smaller than one. Further increase of the free-stream Mach number only makes the shock angle smaller without changing its root position.

Position of the surface shock is plotted in Fig. 30 against the transonic similarity parameter together with the theoretical curve by Spreiter [*3*] and the experimental results by Bryson [*6*] both for circular-arc airfoils. In case of the λ-shock the tip shock is artificially extended to the surface and their cross point was taken to be the shock position. In Fig. 30 is clearly seen systematic deviations of the experimental points according to the airfoil thickness parameter τ such that the thinner the airfoil is the faster is the rearward movement of the surface shock. If this is true, it is reasonable that all of the experimental points, except one, lie in the right hand side of the Spreiter's theoretical curve obtained under the assumption of vanishing airfoil thickness. As far as the shock position is concerned, the experimental results do not seem to confirm the transonic similarity rule.

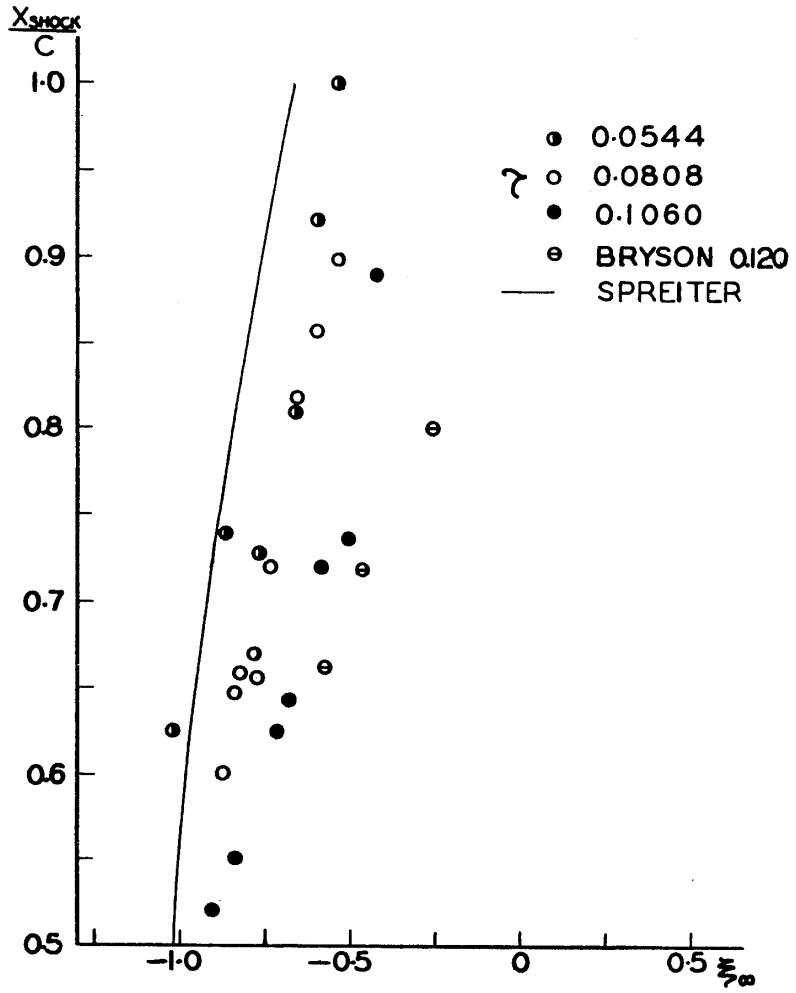

FIGURE 30. Location of surface shock versus transonic similarity parameter.

3. 8 *Location of the Sonic Point and the Root of the Limiting Mach Line*

The most characteristic feature of the transonic flow around the bodies with curved surface like circular-arc airfoils is the movement of the sonic point on the boundary with free-stream Mach number. In the case of a double-wedge section, the sonic point is always fixed at its shoulder. Variation of the sonic point with transonic similarity parameter obtained in the preseut experiment is shown in Fig. 31, in which is given Spreiter's theoretical curve and Bryson's experimental results for comparison. Though distributions of experimental points are widely dispersed because of the error in measurement, the general tendency of the sonic point movement in theory coincides with that in experiment. In the theory, the sonic point locates at the quarter-chord at Mach number one, while, in the present experiment, it seems to lie a few percent ahead of the theoretical value. The same tendency is seen in the experimental result obtained at ONERA as shown in Fig. 16. Also the stationary state of the sonic point location at $M_\infty=1$ is not certain from the experiment.

Obtaining the transonic flow field around a two-dimensional body by experiment, we can compose the boundary of the flow in the hodograph plane. Such

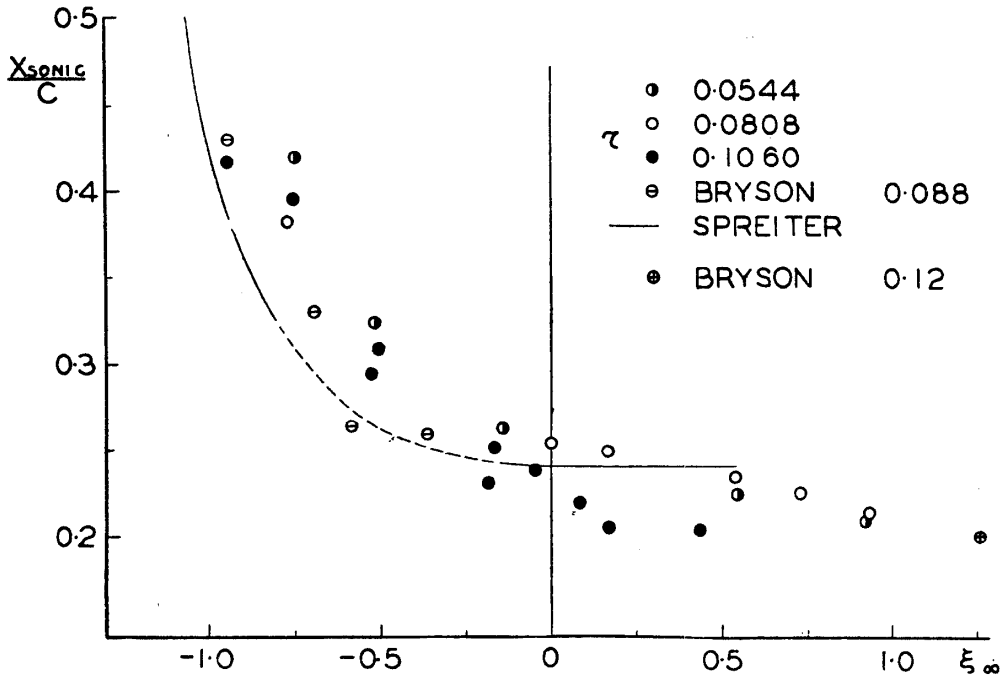

FIGURE 31. Variation of sonic point on the airfoil surface at zero incidence with transonic similarity parameter.

hodograph boundaries are shown in Fig. 32 for three kinds of circular-arc airfoils used in the present experiment at Mach numbers nearly equal to one. In this figure, θ is the flow direction angle in radian, θ_0 the flow direction angle at the leading edge and η the non-dimensional perturbation velocity defined as

$$\eta=(\gamma+1)\frac{w-w^*}{w^*},$$

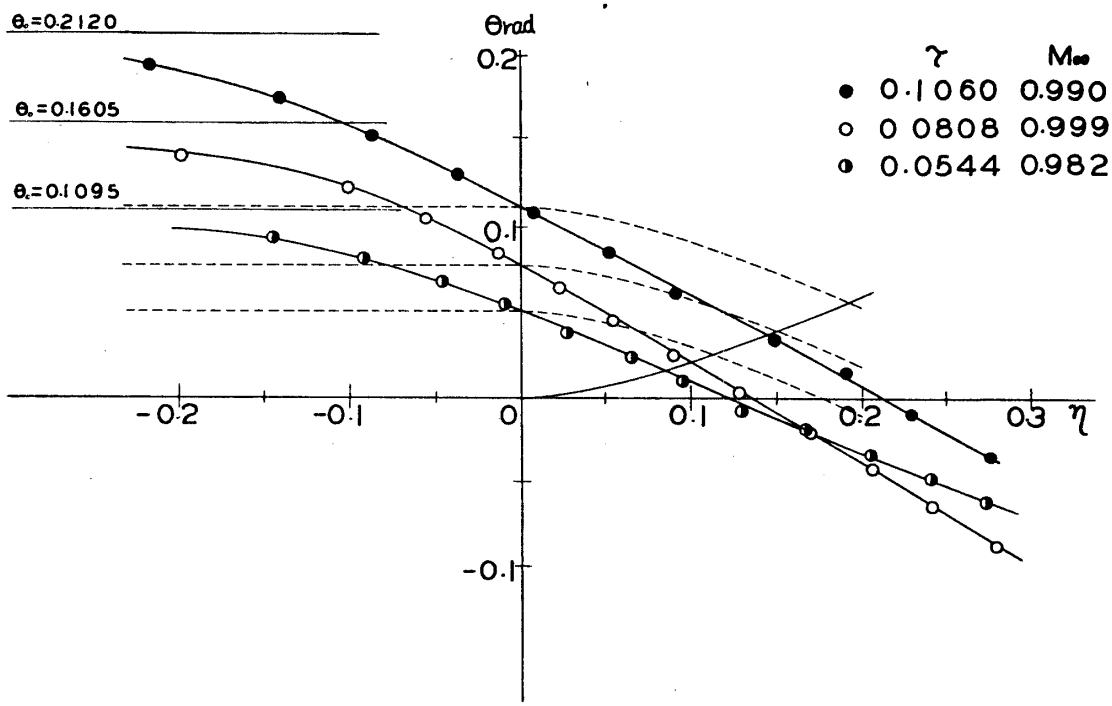

FIGURE 32. Hodograph boundaries for three kinds of circular-arc airfoils at $M_\infty \doteqdot 1$, $\alpha=0°$.

where γ is the ratio of the specific heats, w the magnitude of the flow velocity and asterisk denotes the critical value. In Fig. 32 is shown with dotted lines the hodograph boundaries of the flow at Mach number one around wedge sections with semi-vertex angle equal to the flow direction angle at the sonic point of the corresponding circular-arc airfoil. It is seen in the figure that, in the supersonic region, the flow seems to be accerlerated linearly with respect to θ thus giving the experimental evidence to the Spreiter's assumption of local linearization theory.

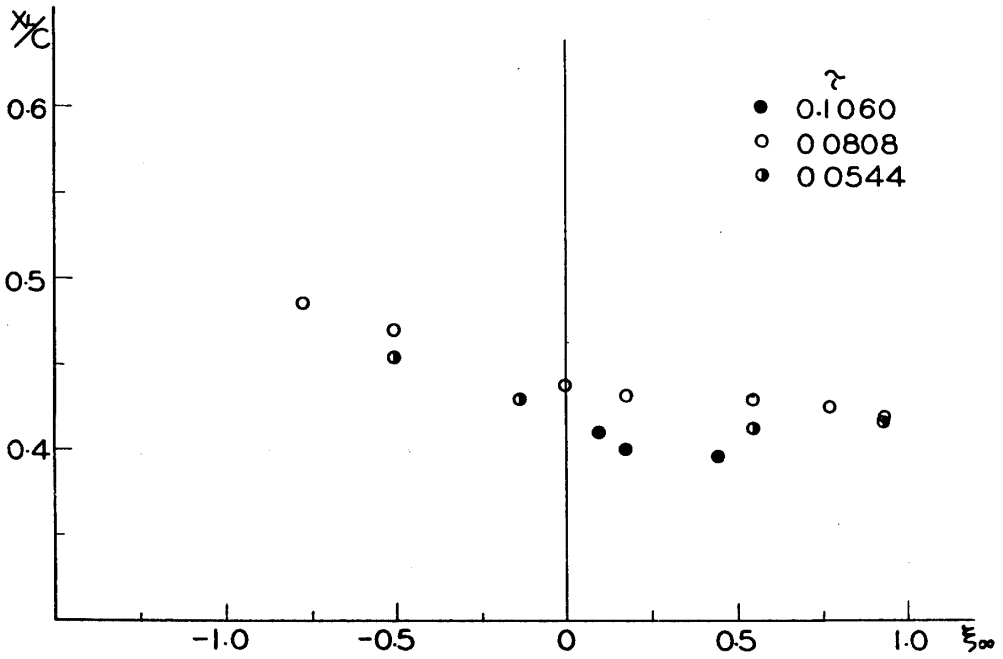

FIGURE 33. Variation of the root of the limiting Mach line versus transonic similarity paramer.

In Fig. 33 is presented variation of the root of the limiting Mach line, which is, for characteristic feature of the transonic flow around the bodies with curved surface, another point of interests. It can be obtained as the intersection of the experimental boundary with the characteristics starting from the origin in the hodograph plane as shown in Fig. 32. Examination of the figure reveals that, in spite of scattering of the experimental points caused by the same reason as in the case of the sonic point location, they have a general trend to retire to 50 percent chord with decreasing free-stream Mach numbers. At Mach number one the root of the limiting Mach line is at about 43 percent chord and it is almost stationary with increasing Mach numbers in the range of the present measurement.

3. 9 *Position of the Detached Shock*

At low supersonic Mach numbers a detached bow shock appears ahead of the leading edge. It is almost normal to the free-stream and has a very small curvature in the present experimental range. Fig. 34 shows variation of the shock-detachment distance measured from the leading edge on the centre line with transonic similarity parameter. It is seen that the experimental points for the airfoils

with different thickness are well arranged in one curve and continue smoothly to the results by Bryson [*6*].

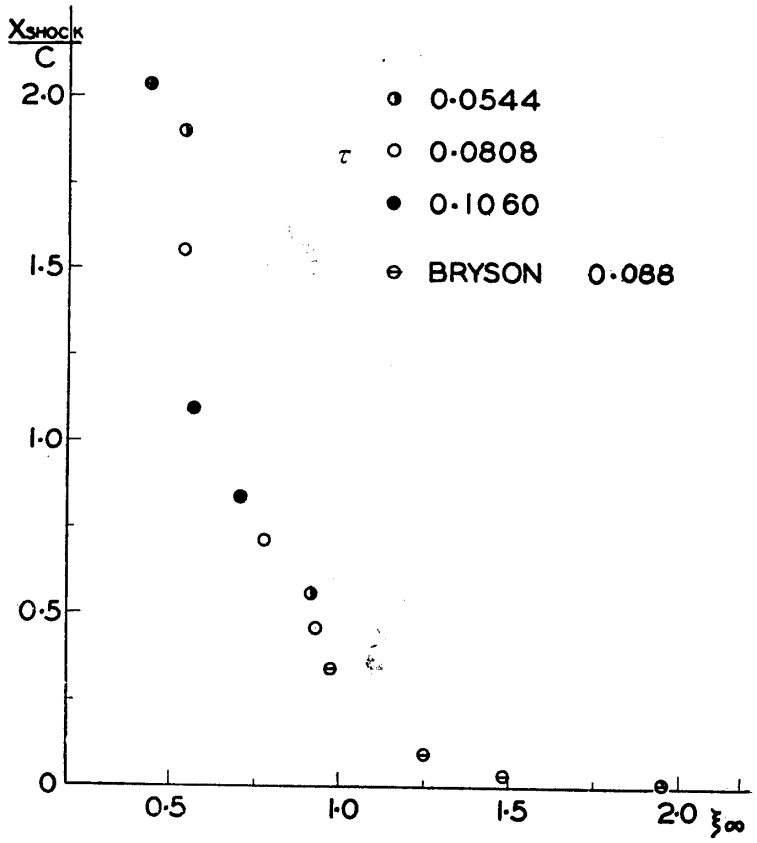

FIGURE 34. Shock-detachment distance at $\alpha=0°$ versus transonic similarity parameter.

It is suggested by Busemann [*13*] that, in the transonic flow with detached shock, the body profile does not everywhere contribute equally to the determination of the flow field. According to his theory, the body boundary near the sonic point has predominant effect on the whole flow field and the boundary near the leading edge or near the stagnation point is relatively unimportant in spite of the position being nearest to the detached shock in the physical plane. It can be intuitively deduced from this suggestion that the essential part of the subsonic flow field behind the detached shock for any slender symmetric airfoil would be simulated by the one for an appropriate wedge section, and the same location of the detached shock would be expected for both flows.

In order to check the above deduction, three kinds of wedge section are taken into consideration for one corresponding circular-arc airfoil. These are, as shown in Fig. 35, two wedges with semi-vertex angle equal to the half of the leading edge angle of the circular-arc airfoil and equal to the flow angle at the sonic point of the circular-arc airfoil and a wedge composed of two straight lines connecting the leading edge and the sonic points of the circular-arc airfoil. In comparing these sections modification of the thickness parameter, $\tau=(t/c)$, is necessary. Here, we take as t half of the maximum thickness for the wedge and half of the thickness at the sonic point for the circular-arc airfoil and also take as c the length of the

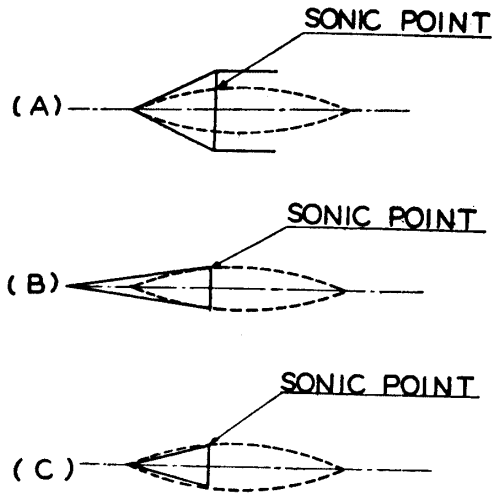

FIGURE 35. Illustration of the modified wedges.

wedge and that from the leading edge to the sonic point for the circular-arc airfoil. By the use of this modified thickness parameter the transonic similarity parameter ξ_∞ is to be replaced by ξ'_∞ defined as

$$\xi'_\infty = \frac{M_\infty^2 - 1}{[(\gamma+1)(t/c)]^{\frac{2}{3}}},$$

where t and c are given by the above mentioned definition.

Location of the detached shock of the wedge sections at low supersonic Mach numbers was obtained by Bryson [6] experimentally and by Vincenti and Wagoner [15] theoretically. Together with these results are shown in Figs. 36 to 38 the data on the shock-detachment distances in the present experiment. In these figures, the ordinate denote the non-dimensional shock-detachment distance D/C and the definitions of D and C for the circular-arc and the corresponding wedge sections are given in each figure. The best arrangement of the experimental points for the

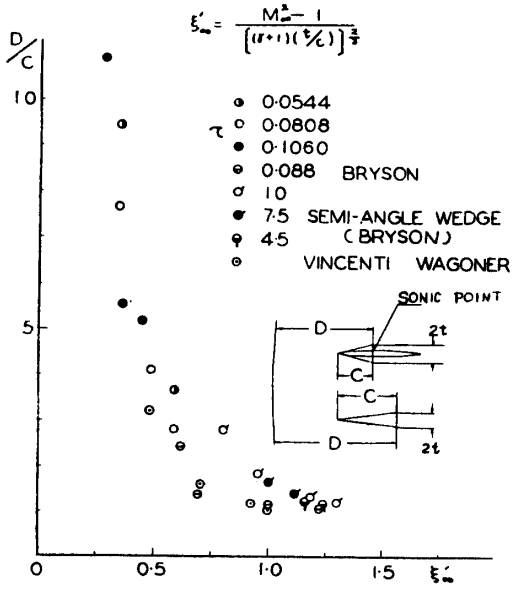

FIGURE 36. Modified shock-detachment distance for modification (A).

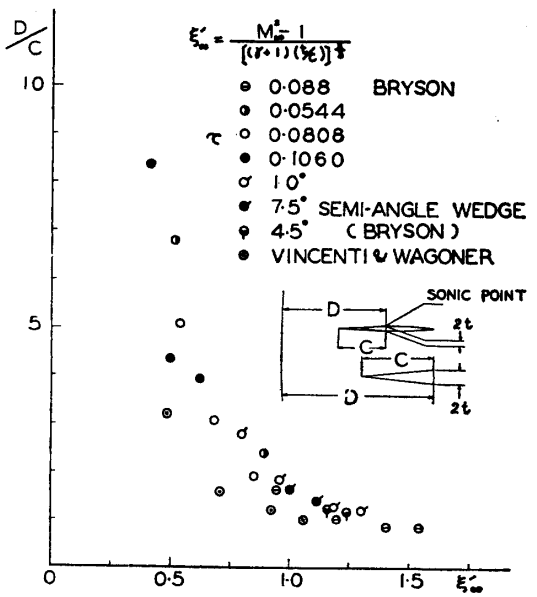

FIGURE 37. Modified shock-detachment distance for modification (B).

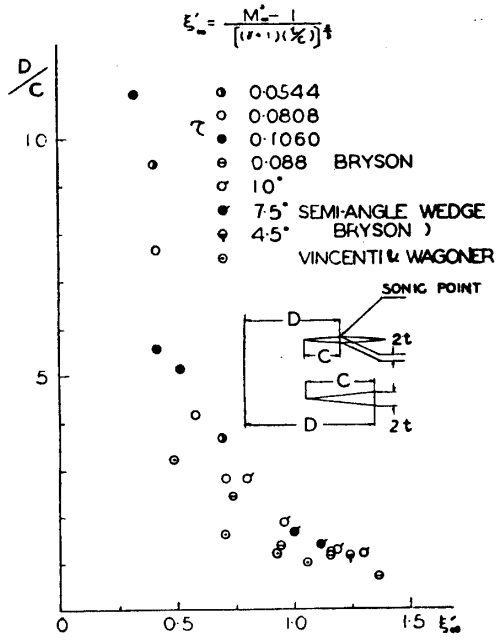

FIGURE 38. Modified shock-detachement distance for modification (C).

circular-arc and the wedge sections by the modified transonic similarity parameter ξ'_∞ is seen in Fig. 37, in which comparison is made between the circular-arc airfoil and the corresponding wedge composed of two tangents at the sonic points on the original airfoil. This fact seems to give an experimental evidence to Busemann's theory that the transonic flow field is most seriously affected by the boundary near the sonic point. In these figures, the theoretical points obtained from the calculation by Vincenti and Wagoner deviate from the experimental ones. This may be caused by the wind tunnel wall interference, though not clear.

4. CONCLUSION

Transonic flow around biconvex circular-arc airfoils has been investigated in a small scale transonic wind tunnel by the use of a Mach-Zehnder interferometer. Aerodynamic characteristics of the airfoils at transonic Mach numbers and at small angles of attack have been calculated from the surface pressure distributions obtained by interferometry. The experimental results have mostly been arranged in the form suitable for the application of the transonic similarity rule. It has been found that lift coefficient of the airfoils is not exactly proportional to angle of attack in the vicinity of free-stream Mach number one. Busemann's reasoning of the transonic flow with detached shock has been confirmed by the analysis of the detached shock location obtained in the experiment.

It must be remarked that the present results pertain to the particular case of laminar bundary layer for the reason that the Reynolds number of the present experiment is low. The presence of turbulent boundary layer would probably lead to other results of experiment. Since the turbulent boundary layer would give

rise in particular to a more remarkable effect of shock wave, it would modify the essential characteristics of the flow phenomena revealed in the present experiment.

Department of Aerodynamics
Aeronautical Research Institute
University of Tokyo, Tokyo
March 4, 1959

References

[1] Guderley, G. and Yoshihara, H.: The Flow over a Wedge Profile at Mach Number 1. A.F. Technical Report No. 5783, 1949.
[2] Gullstrand, T. R.: The Flow over Symmetrical Aerofoil without Incidence in the Lower Transonic Range. KTH-AERO TN 20.
[3] Spreiter, J. R. and Alksne, A.: Theoretical Pressure Distributions for Several Related Non-Lifting Airfoils at High Subsonic Speeds. NACA TN 4148, 1958.
[4] Maeder, P. F.: Solutions to the Linearized Equation for Transonic Flows and Their Comparison with the Experiment. USAF 18 (600)-664.
[5] Spreiter, J. R., and Alksne, A.: Thin Airfoil Theory Based on Approximate Solution of the Transonic Flow Equation. NACA TN 3970, 1957.
[6] Bryson, A. E.: An Experimental Investigation of the Transonic Flow Past Two-Dimensional Wedge and Circular-Arc Sections Using a Mach-Zehnder Interferometer. NACA Rep. 1094, 1952.
[7] Spreiter, J. R.: Similarity Laws for Transonic Flow About Wings of Finite Span. NACA TN 2273, 1951.
[8] Spreiter, J. R.: On the Application of Transonic Similarity Rules. NACA TN 2726, 1952.
[9] Michel, R. R., and Sirieix, J. J.: An Experimental Contribution to the Study of the Lifting Airfoil at Transonic Speeds. ONERA.
[10] Vincenti, W. G., and Wagoner, C. B.: Theoretical Study of the Transonic Lift of a Double-Wedge Profile with Detached Bow Wave. NACA TN 2832, 1952.
[11] Cole, J. D., Solomon, G. E. and Willmarth, W. W.: Transonic Flow Past Simple Bodies. J.A.S. No. 9, Sept., 1953.
[12] Guderley, G., and Yoshihara, H.: Two-Dimensional Unsymmetric Flow Patterns at Mach Number 1. J. A. S. November, 1953.
[13] Busemann, A.: A Review of Analytical Method for the Treatment of Flows with Detached Shocks. NACA TN 1858, 1949.
[14] Michel, R., Marchaud, F., and Le Gallo, J.: Etude des ecoulements transsoniques autour des profils lenticulaires, a incidence nulle. ONERA. Pub. No. 72, 1954.
[15] Vincenti, W. G., and Wagoner, C. B.: Transonic Flow Past a Wedge Profile with Detached Bow Wave. NACA TR 1095, 1952.